Atomic Force Microscopy (AFM)

Yinan Liu, Tolga Atalay
Advanced Master Lab, summer semester 2022
Department of Physics, Freie Universität Berlin

Abstract

In this experiment, a Nanotec AFM was employed to investigate surface topography of gold islands on highly oriented pyrolyric graphite (HOPG) as well as gold islands on Si(111) evaporated through masking polystyrene spheres. Voltage spectroscopy without feedback was performed on the gold and HOPG sites to determine the contact potential of these regions. Voltage spectroscopy with constant force gradient feedback characterized the shape of the AFM tip to be best described with a sphere. A crash occurred to the tip at the end of investigating the first sample. Using the crushed tip in the contact regime, we were nonetheless able to obtain high quality surface scan of the second sample showing distinct periodicity as well as hexagonal geometry of the gold islands surrounding the polystyrene sphere.

Theoretical Background

The development of the scanning tunneling microscopy (STM) in 1981 by Binnig and Rohrer allows the probe of surface topography with atomic precision by utilizing the tunneling current between the microscope tip and the sample[1]. However, its limitation to the class of conductive, or semiconductive materials led to the development of atomic force microscopy (AFM) in order to investigate other surfaces ranging from insulators to biological samples. Not only does AFM have the advantage of being able to scan almost any sample as an imaging tool, but it also can perform spectroscopic investigation of the surface at the nanometer scale.

In 1986, Binnig, Quate and Gerber reported their development of the first AFM by replacing the tunnelling probe of an STM with a lever made from a small diamond glued onto the end of a thin strip of gold[2]. Modern AFM typically consists of a cantilever with a small tip attached to the free end, a laser, a position sensitive photodetector, and a piezo controlled scanner (Figure 1). The tip is often less than 100 angstroms in diameter and a few microns long. The length of the cantilever can range from 100 to 200 μm.

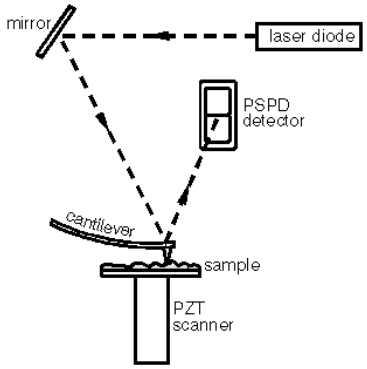

Figure 1. Schematic of beam bounce detection in an AFM. [3]

In this set up, a laser beam deflects from the back of the cantilever to a position sensitive photodetector (PSPD). The position of the laser into the PSPD changes as the height of the cantilever shifts. This allows for the detection of the vertical movement of the tip within the sub-angstrom range[4].

A few different forces between the tip and the sample causes the deflection or the bend of the cantilever:

$$F_{total} = F_{chem} + F_{vdW} + F_{elec} + F_{mag}$$

Eq. 1

Where F_{chem}, F_{vdW}, F_{elec}, F_{mag} are short-range chemical force, van der Waals interaction, electrostatic force, and magnetic force, respectively. F_{mag} is only relevant for magnetic tips and samples, and therefore can be disregarded in this experiment.

The electrostatic potential in AFM comes from the tip and the sample forming a capacitor when an applied voltage is present, and can be described as:

$$F_{elec} = \frac{1}{2}\frac{\partial C}{\partial z}V_{eff}^2$$

Eq. 2

here C is the tip-sample capacitance, V_{eff} the applied voltage, which is the sum of the bias voltage V_{bias} and the contact potential V_{CPD} where:

$$V_{CPD} = (\phi_{Sample} - \phi_{Tip})/e$$

Eq. 3

The contact potential is sample dependent as it results from the difference between the work function of the sample and the tip[5]. This relationship allows the spectroscopic investigation of the sample, where the distance-voltage curve also depends on the geometry of the tip in the constant force gradient regime[6].

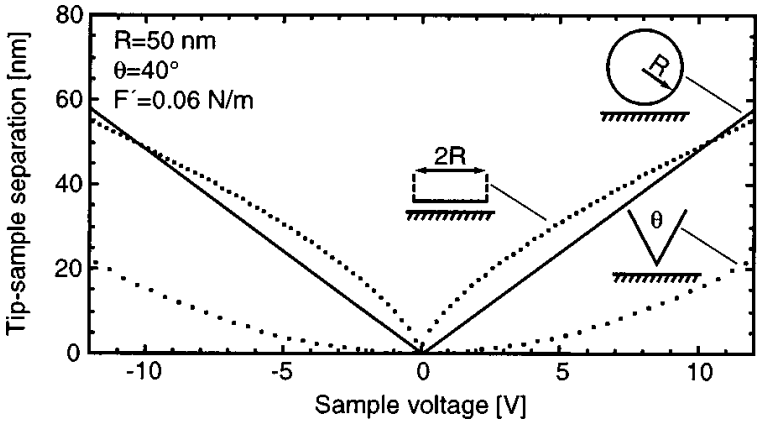

Figure 2. Theoretical relationship between tip-sample separation and sample voltage with various tip shape under constant force gradient regime[5].

As the distance between the tip and the sample, and the contact regime of the AFM varies, different interatomic forces are at play. The following sections will discuss the two main distance modes, contact regime and non-contact regime in detail.

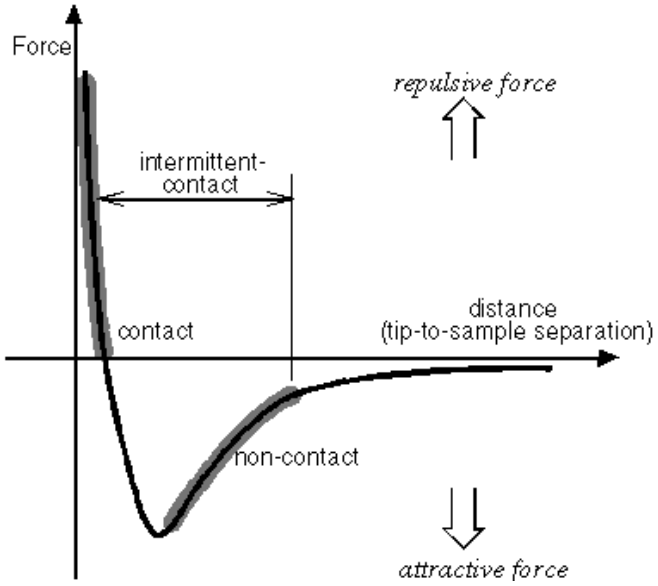

Figure 3. Interatomic force vs. distance between tip and sample profile. [4]

Contact AFM

The contact AFM regime is also known as the repulsive mode since the dominating interatomic force at play is the repulsive short-range forces as shown on the left side of the force vs. distance curve (Figure 3). The cantilever is within less than a few angstroms of distance from the surface. As the atoms are brought closer together within the distance of a couple angstroms, the negatively charged electron clouds begin to repel each other as a result of Pauli exclusion-principle repulsion. The repulsive and attractive interactions at small distance ranges is described by a simple Leonard Jones potential U_{LG}:

$$U_{LG} = 4\varepsilon\left[\left(\frac{\sigma_o}{r}\right)^{12} - \left(\frac{\sigma_o}{r}\right)^{6}\right]$$

Eq. 4

where σ_o is the distance at which the potential is zero, r is the distance between the two interacting atoms, and ε is the strength of the potential at its minimum[3]. The distance at which the potential is at its minimum is $r = 2^{1/6}\sigma$. This relationship describes that atom repel each other at small distances, and the strength of this force weakens until the attractive forces dominate when atoms reach a moderate distance. The term $\left(\frac{\sigma_o}{r}\right)^{12}$ describes Pauli repulsion whereas $\left(\frac{\sigma_o}{r}\right)^{6}$ models the attractive forces between molecules, generalized by the term van der Waals interactions. It can be characterized into two categories: the Dipole-dipole forces among

permanently polar molecules, and the London dispersion forces among temporary dipoles. Molecules can have permanent dipoles due to the difference in the atom's electronegativity, as well as temporary ones as a result of the changing charge distribution in a non-polar molecule. Since the Leonard Jones potential describes the short-range forces felt between two atoms, in order to describe the interactions that are felt by other adjacent atoms on the sample as well as the general tip, we use another term, F_{vdW}, to describe the attractive electrostatic force felt between the tip and the sample. It can be expressed by approximating the tip atoms involved in this interaction as a sphere in front of a surface that is infinitely extended:

$$F_{vdW} = \frac{HR}{6d^2}$$

Eq. 5

where H is the Hamaker constant, R is the radius of the tip, and d is distance between the tip and the sample. In the case where water is present in ambient environment, a capillary force that arises from thin water layer which holds the tip in contact with the surface also needs to be considered.

Two modes can be operated in the contact AFM regime: constant height mode or constant force mode, analogous to the two modes used commonly in STM. In constant height mode, the scanner is held at a fixed heigh above the sample, and the deflection of the cantilever can be directly used to generate surface topography data. This mode is commonly used to achieve atomic resolution. In constant force mode, a piezo modulated feedback loop keeps the cantilever's deflection constant, therefore keeping the force applied to the sample constant[4].

Non-contact AFM

In non-contact AFM regime, the cantilever's position on average is at the order of tens or hundreds of angstroms from the sample surface. The cantilever used also has a stiffer spring constant than that used in the contact AFM regime to prevent the cantilever being pulled into contact with the surface of the sample. The atomic force between the sample and the tip is generally very low. Instead, the cantilever is vibrated near its resonant frequency, and the change of the frequency is monitored as the tip scans through the surface.

We can use the model of a damped harmonic oscillator with forced oscillation to model the cantilever's oscillation:

$$m\ddot{z} + \gamma\dot{z} + kz = F_o cos(\omega t) + F_{total}$$

Eq. 6

where m is the mass, z the distance between the tip and the sample, γ is the damping of the oscillation, k the spring constant, and $F_o cos(\omega t)$ describes the oscillation in the piezoelectric element. From this relationship, assuming F_{total} is zero, or kept constant, we can obtain the free oscillation frequency:

$$\omega_o = 2\pi f_o = \sqrt{\frac{k}{m}}$$

Eq. 7

The interaction between the tip and the sample will then cause a change in the effective spring constant of the system:

$$k_{eff} = k - \frac{\partial F_{total}}{\partial z}$$

Eq. 8

As a result, the new resonant frequency is shifted by:

$$\Delta\omega_o = -\frac{\omega_o}{2k}\frac{\partial F_{total}}{\partial z}$$

Eq. 9

where the force gradient is described by the change in amplitude:

$$\frac{\partial F_{total}}{\partial z} = k\left(\frac{1 - 2a^2 + \sqrt{4Q^2(a^2 - 1) + 1}}{2(Q^2 - a^2)}\right)$$

Eq. 10

a is the ratio between the amplitude of the free resonance and the feedback amplitude, and Q is the quality factor[3].

In the no-contact regime, the piezo controlled feedback loop keeps the resonating frequency of the cantilever constant by changing the height of the scanner. This motion can then generate data about surface topography. Non-contact AFM does not suffer from degradation of the tip or the sample in comparison to contact AFM. It is also superior to contact AFM in scanning soft surfaces, or where liquid layer is present (Figure 4).

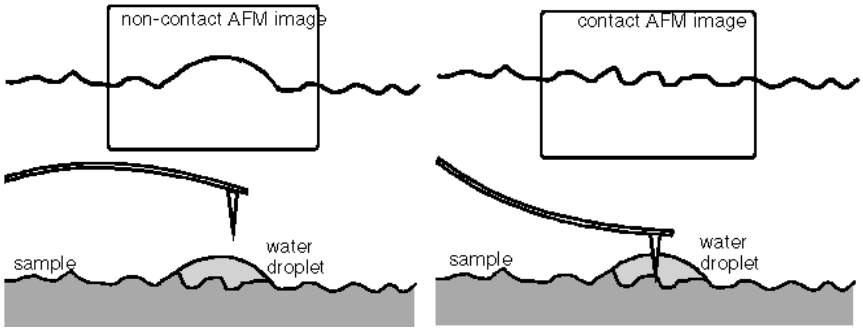

Figure 4. Contact vs. non-contact AFM in scanning a surface where water droplet is present. [4]

Experimental Set up

The experimental set up consists of an AFM, and a computer with digital signal processing to control the AFM. In this experiment Nanotech AFM is used. The two main components, head and chassis of the AFM is shown in Figure 5 and Figure 6 respectively.

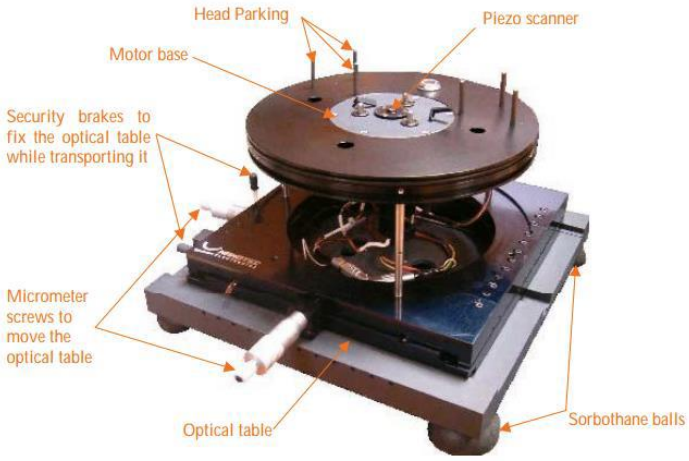

Figure 5. Chassis of the Nanotech AFM [7].

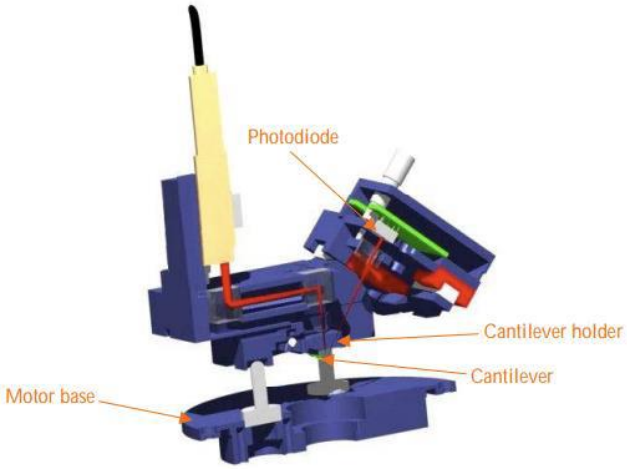

Figure 6. SFM head cross section [7].

The chassis of the AFM holds the piezo sample holder, motor base and the micrometer screws to move the optical table. Cantilever holder, photodiode, and the laser are mounted on the SFM head, which also contains screws for calibration of the photodiode.

Experimental Procedure

To start the experiment, a fresh cantilever is mounted on the AFM head. The laser is then tuned so that the beam is focused on the cantilever by adjusting the screws for laser alignment. Next, the photodiode is tuned so that the laser reflected from the cantilever is centered. The "Tune photodiode" option is selected on the computer program and with the indication from the photodiode signal shown in this program, the photodiode is centered. After alignment is accomplished, Sample A (Au on highly oriented pyrolytic graphite (HOPG)) is mounted on sample holder and AFM-head is installed.

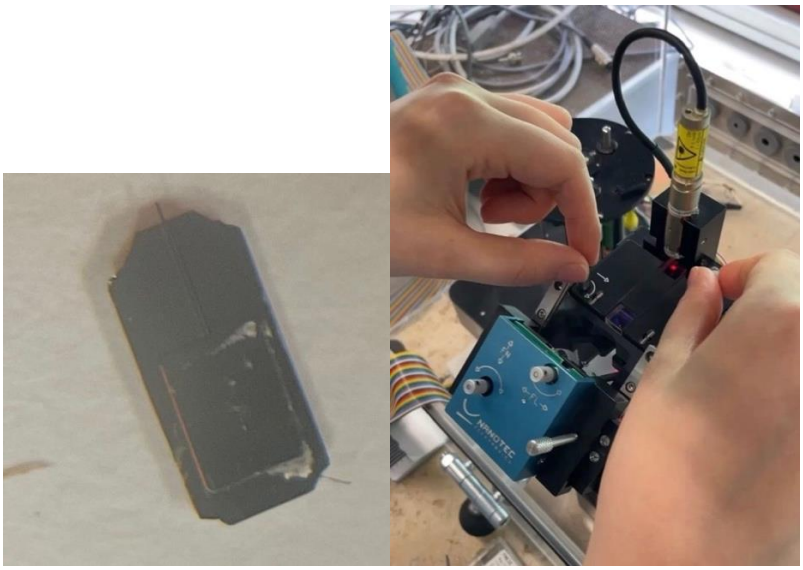

Figure 7. Left: AFM cantilever used in the experiment. Right: The laser beam is being focused onto the cantilever.

First, the resonant frequency of the cantilever is determined by reducing the oscillation amplitude to approximately 1V. The tip is then approached the sample with the oscillating amplitude decreased by 25%. We proceeded to scan the surface of Sample A with the goal of locating a region that will be suitable for spectroscopy measurements later.

After the topography of this region that has clear gold and graphite islands is acquired and saved, we proceeded to conduct voltage spectroscopy of 10 locations on both graphite and gold region. IV Spectroscopy window on AFM control software is opened and appropriate values are set in this dialog window. For voltage spectroscopy without feedback, "feedback on during ramp" is set off. AFM tip is then placed on various points of the gold island and the graphite substrate. A total of 20 voltage spectra ranging from -2000 mV to +2000mV is taken and saved.

Next, voltage spectroscopy is taken with feedback. For this purpose, "feedback on during ramp" is set on in the IV Spectroscopy window. The unit of the topography recording channel is set to nm and number of points per spectrum is set at 256. With the tip placed on a point on the graphite surface, voltage spectrum is taken with voltage is ramped through -9.5V to +9.5V. This spectrum with feedback was taken at 10 different points on the graphite substrate. After the third spectra was taken on the gold island region, a crush of the STM tip occurred during the process. Since this part of the experiment is conducted for the qualitative analysis of the STM tip shape and we already had 13 successful spectra, we decided to terminate this part of the experiment and proceed to scanning the next sample.

Sample A is then removed after withdrawing the tip using "withdraw" button in "approach" window and turning off the laser in "photodiode" window. Sample B is installed, and AFM is aligned again using the same method of preparation for sample A. Using the crushed tip from the previous part of the experiment, an area of Sample B of the size $20x20\mu m^2$ is scanned and saved under contact mode. Through changing the resolution and scan rate, we zoomed into one "unit cell" structure of sample B to acquire more detail and saved this image to the computer as well.

Results

Resonance curve and characteristics of the cantilever are determined using AFM software and shown in Figure 8 and Table 1.

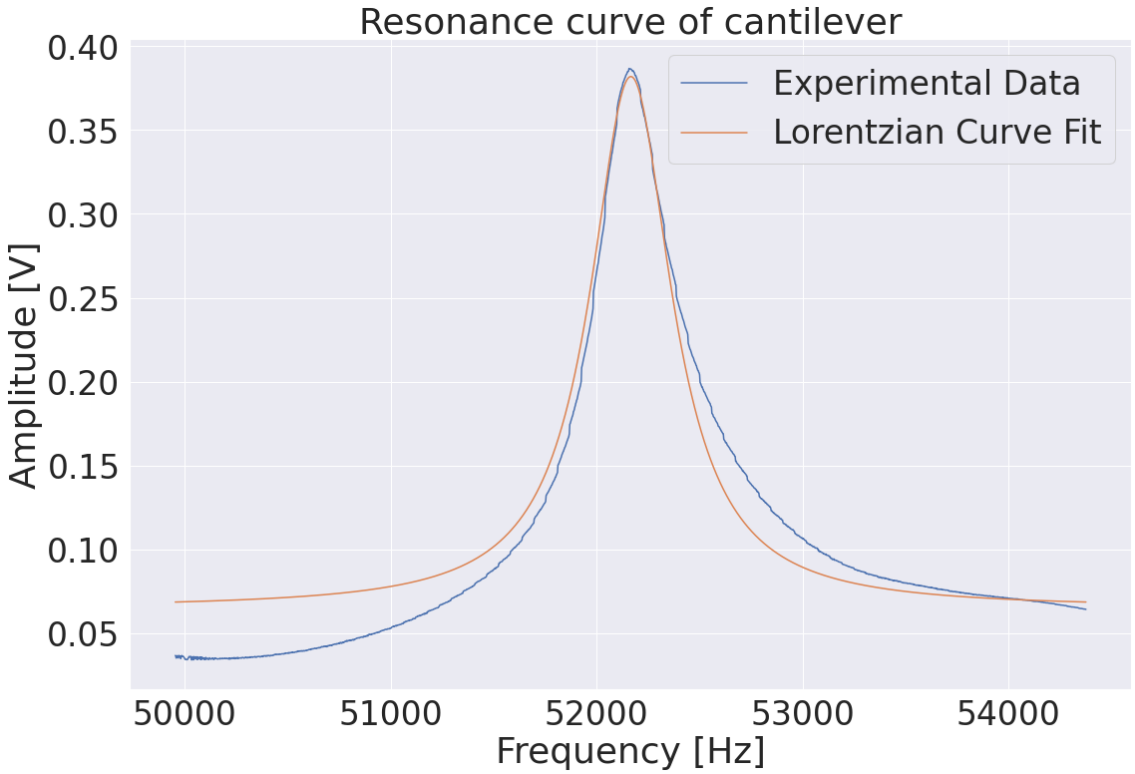

Figure 8. Resonance curve of the cantilever used in this experiment.

Bandwidth	310.339
Quality Factor	168.095
Resonance Frequency	52159.8 Hz
Force Constant	1.40893 N/m

Table 1. Cantilever parameters.

Sample A (Au on HOPG) topography is mapped by scanning an area of size $5x5\mu m^2$ in non-contact mode and shown in Figure 9.

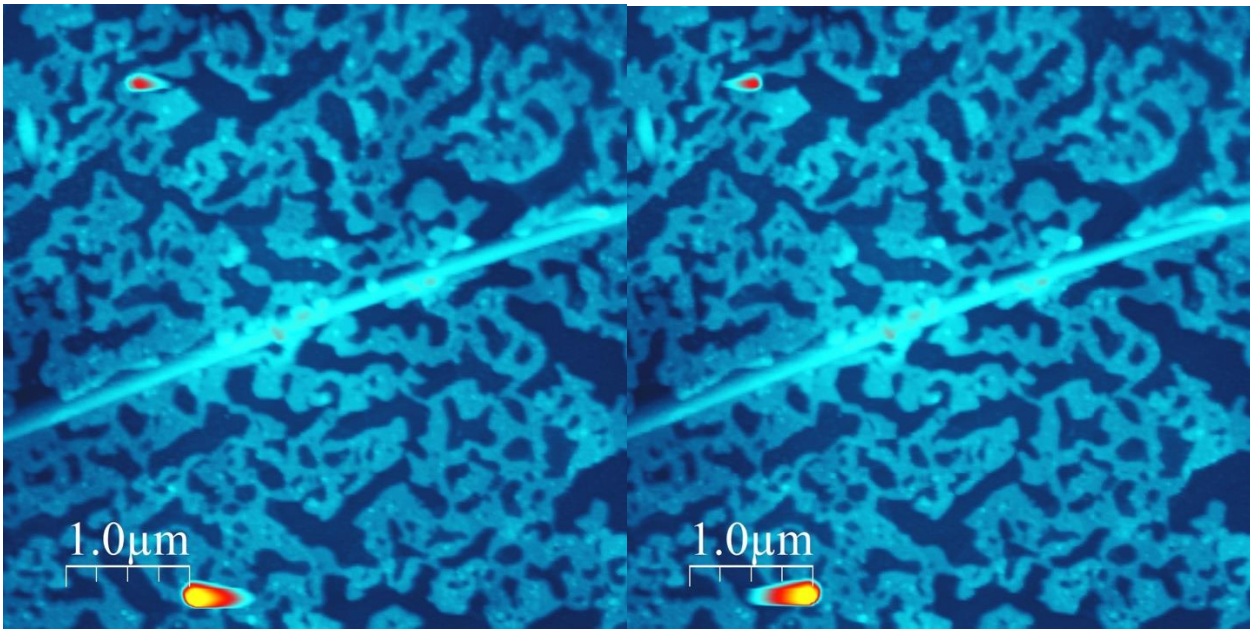

Figure 9. Left: Forward scan of the Sample A. Right: Backward scan of the Sample B.

Voltage spectroscopy of 10 different points on HOPG and Au islands are obtained by averaging 10 voltage spectra on each point.

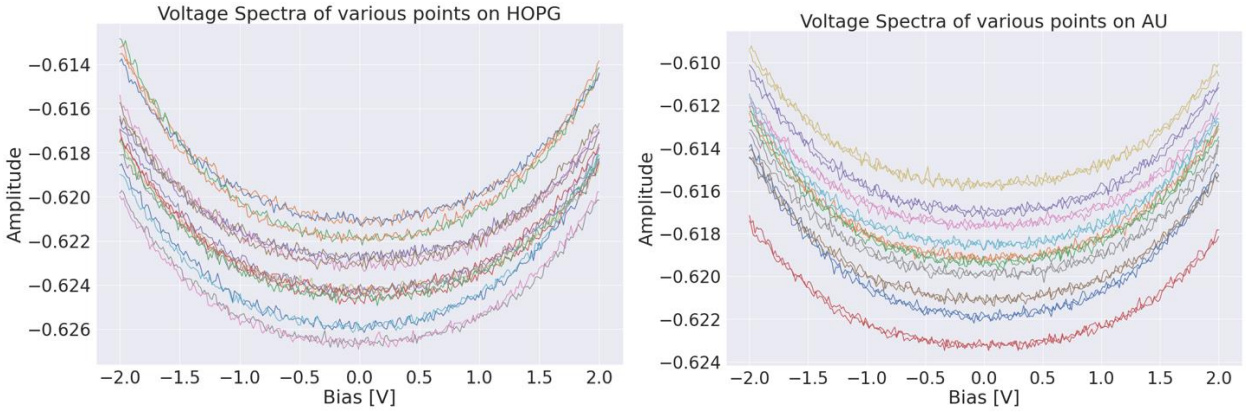

Figure 10. Left: Voltage Spectra of HOPG. Right: Voltage Spectra of AU.

By fitting each voltage spectra to formula $Amplitude = \frac{\partial c}{\partial z}\left(V_{bias} + V_{cpd}\right)^2 + Offset$ and averaging fitting parameters, V_{CPD} for HOPG and AU is obtained:

$$V_{CPD}(HOPG) = 0.0585 \pm 0.00280$$
$$V_{CPD}(AU) = 0.0676 \pm 0.00565$$

Parabolic fit of voltage spectra using mean fitting parameters shown in Figure 11.

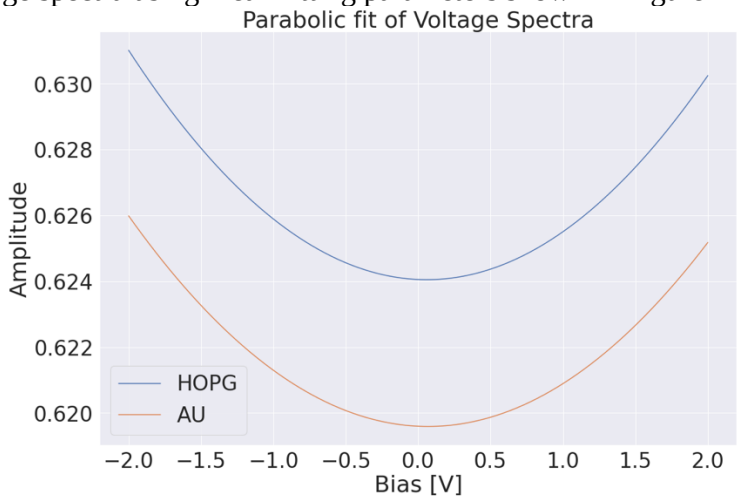

Figure 11. Parabolic fit of voltage spectra.

Voltage spectroscopy with feedback is then performed on a point on HOPG and on an Au island.

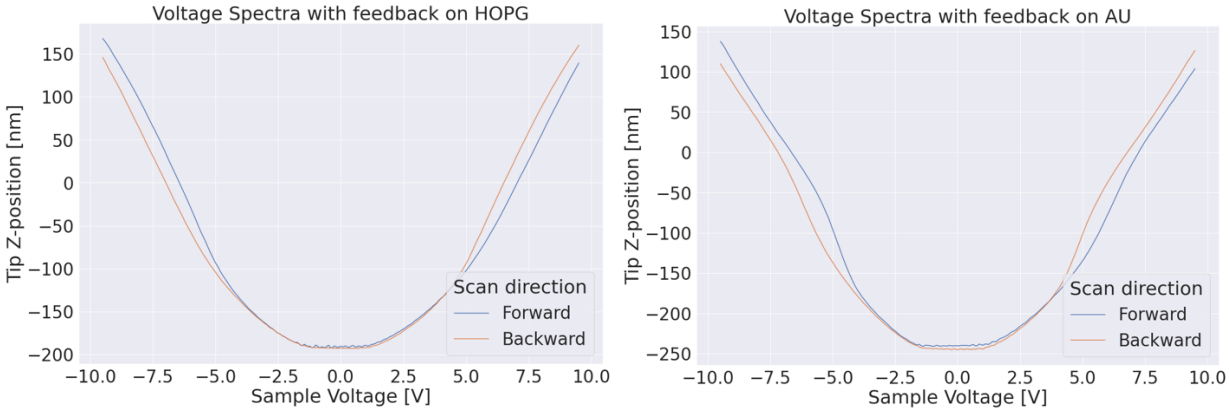

Figure 12. Voltage Spectra with feedback on HOPG and AU.

Tip shape determination

Figure 13 shows 3 tip shape approximations, cone, sphere, and planar, using voltage spectra with feedback data on HOPG and Au islands. Tip shape determination and the fitting of our data is calculated using the in-situ method described by Olsson et al. [6]

Voltage spectra with feedback are obtained at points on HOPG and Au islands. Constant force gradient to regulate sample position with respect to voltage between tip and sample is calculated using equation 10. A0 is set to -1V during scanning process and the value for set point (A) is 0.6V. Quality factor (Q) of 168.095 and Force constant (k) of 1.41 N/m are obtained from image file.

Using the parameters set during experiment and experimental data, constant force gradient used to regulate IV feedback is determined to be 0.011N/m using equation 10.

Since Interactions between tip and sample in lower voltages are mainly due to van der Waals interaction, to consider tip shape where electrostatic interaction take place, current voltage data for sample voltages $|U| > 3V$, where electrostatic forces dominate are used in the numerical methods for fitting. It is noted that fittings are centered around 0.280V, where a shift is observed due to contact potentials.

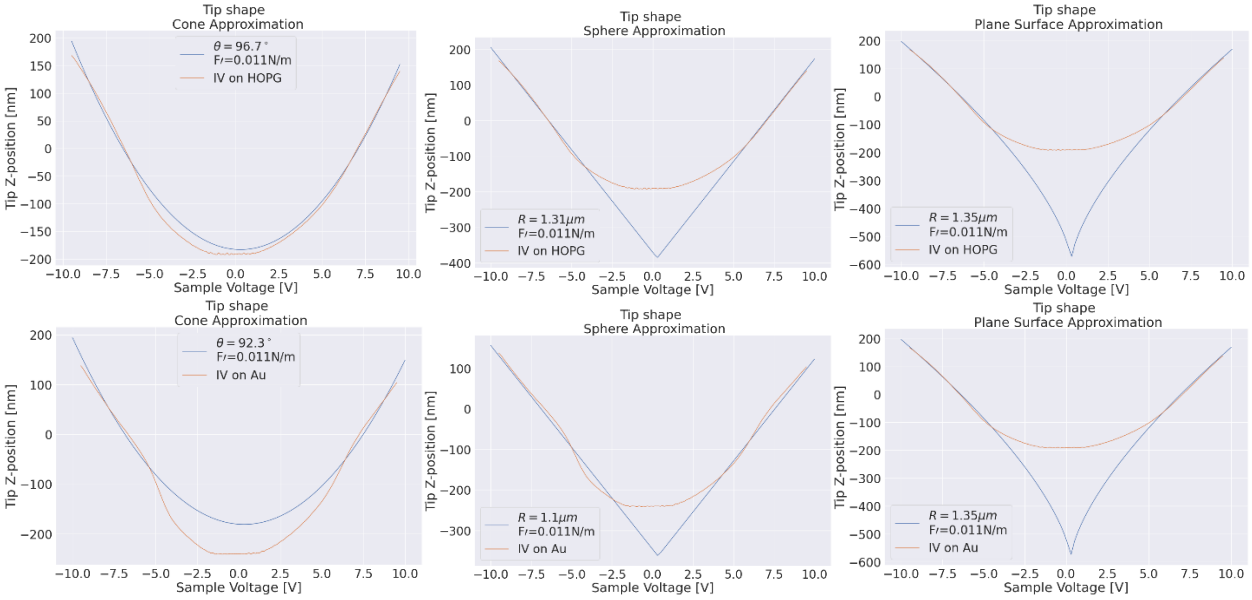

Figure 13. Top: AFM tip geometry approximation using IV spectra on HOPG, Bottom: AFM tip geometry approximation using IV spectra on Au.

From our numerical methods, the sphere shape approximation generated the highest R^2 values of 0.99 on HOPG and 0.96 on Au islands, where the flat shape approximation yielded R^2 values of 0.93 on HOPG and 0.94 on Au islands, and the cone approximation generated R^2 values of 0.95 on HOPG and 0.98 on Au islands.

The cone angle approximated using the conical fitting generated a cone angle of 96.7 degree on HOPG surfaces, and 92.3 degree on au islands. In the spherical approximation of the tip shape,

radius obtained from the data on HOPG is 1.31 um, and 1.1 um on Au islands. In the planar approximation of our tip, data obtained on HOPG yielded a planar radius of 1.35 um, and from Au islands 1.35 um.

During IV spectroscopy with feedback on an AU island, AFM tip is crashed into the sample. Topography of Sample B is determined by scanning the sample in contact mode.
Scan of an area of the size $40x40\mu m^2$ on Sample B surface and a close-up scan are shown in Figure 14.

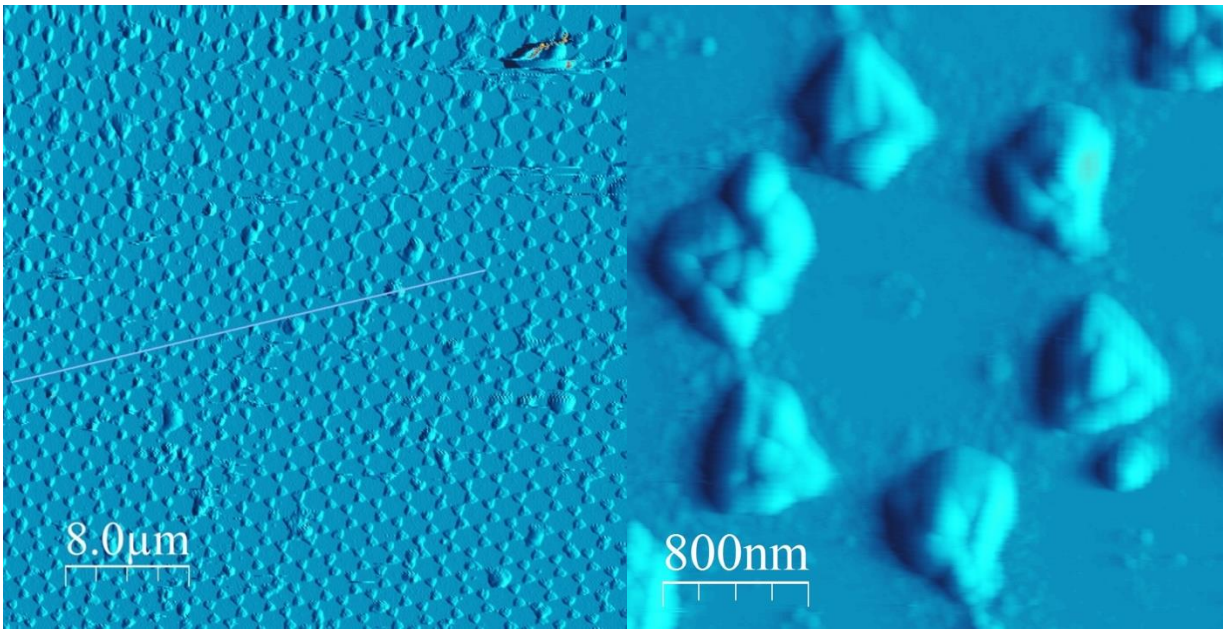

Figure 14. Left: Surface topography of Sample B. Right: Close up scan showing gold deposited through gaps between mask of polystyrene spheres..

Diameter of the spherical mask used in deposition process is measured by calculating mean distance of several circular gaps between gold depositions. Distance of the blue line shown in Figure 14 is measured using WSxM software and then divided by the circular gaps it encloses.

$$D_{mask} = 1.833\mu m \pm 0.012\mu m$$

Discussion

The second order polynomial fit of our data points in the voltage spectroscopy without feedback regime indicates that the electrostatic force gradient is dependent on the applied voltage. This relationship is in good agreement with the one described in equation 2.

Now using literature value of the work potential of deposited gold film at 5.30eV[8], HOPG at 4.6eV[9], we would like to calculate the theoretical contact potential at gold and HOPG sites. Assuming the tip's contact potential remains the same throughout the measurement, using equation 3, we would have a theoretical contact potential mean difference between the gold sites and the HOPG sites of $V_{CPD\text{gold}} - V_{CPD\text{hopg}} = 0.70\text{V}$. Our experimental result, $V_{CPD\text{gold}} - V_{CPD\text{hopg}} = 0.0091 \pm 0.0084V$, although showing good consistency and small variance among

10 cycles of measurement at two different sites, does not include the theoretical value within its boundaries of uncertainty.

Although the difference between the mean experimental V_{CPD} of gold and HOPG sites is a positive one, there is not a significant difference between the two as suggested by the theoretical work potentials of deposited gold film and HOPG. We would like to attribute this deviation to contaminants on the surface and our measurement environment. First of all, there are visible white speckles throughout the typography scan of our first sample, suggesting an uncleaned sample surface where dust is present. Secondly, literature work functions of gold and HOPG were measured in vacuum, and our experiment was done in ambient air. Therefore, the ambient environment between the tip and the sample which contained impurities will also interfere with our measurement, causing a reproducible correlation between our experimental contact potential to the work function of the two surfaces to be unlikely.

Using analytical methods provided in Olsson et al [6], we were able to analyze the tip shape used in our experiment in situ both quantitatively and qualitatively. It is important to note that, in order to provide the best fit for the data according to the analytical methods in Olsson et al, regions where electrostatic forces dominate should be used to for the analysis, excluding the data that is generated from the van der Waals interactions between the tip and the sample. The R^2 values generated from the fitting of our data led to the conclusion that our tip shape can be best described with a sphere, with the second highest R^2 score being obtained by a conical shape, and the third being the planar approximation. We also noted that even under the same shape regime of the tip approximation, R^2 values obtained on HOPG and Au surfaces vary. From this we would like to suggest that, in order to have further accuracy on the tip shape, more samples could be used to evaluate tip shape across a variety of surface Similar to the V_{CPD} determination, measurements could be done in vacuum in order to avoid fluctuations due to ambient environment. It is important to recognize that, as mentioned in Olsson et al, this analytic method is best suited for routine checks of tip quality during the experiment without the need to disturb the overall configuration of the AFM set up during the experiment. We believe that in a laboratory set up where more accuracy is required and the measurements are done in vacuum, this method is able to provide a way for investigators to maintain quality control over the tip shape throughout the experiment.

In a piezoelectric material, the ideal relationship between the applied voltage and the extension is a linear one. However, this is rarely the case in real measurements. The intrinsic nonlinearity of piezoelectric materials used in AFM systems will cause the step sizes to be not uniform, therefore contouring linear structures [4].

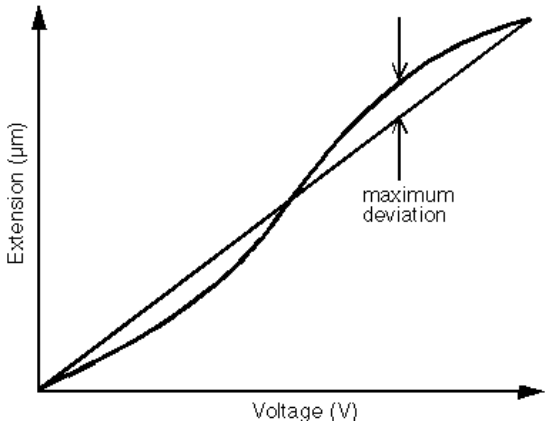

Figure 15. Extension vs. Voltage graph demonstrating nonlinearity in piezoelectric material [4].

Our forward and backward scan of the same region on sample B does not result in the same image, with the backward scan showing significantly more defect sites and smearing. These discrepancies points to the hysteretic behavior of the piezo. Some effect of creep can also be attributed to the discrepancies between the top and bottom spheres in figure 14. When a piezoelectric material is subjected to an abrupt change in voltage, its dimensional change is not instantaneous, but rather takes a long time to occur. The big defect in the top right corner of figure 14 could be resulted the tip dragging impurities on the surface, leading to an unstable feedback regulation in that region, and making the scan appear to be smeared (figure 16).

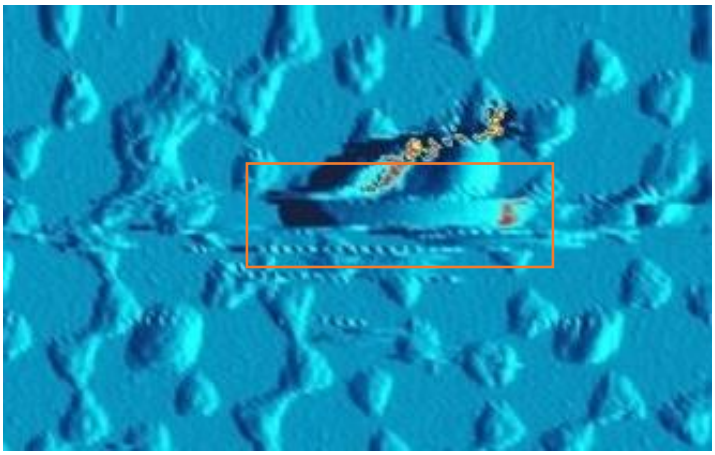

Figure 16. Effects of impurities on the surface.

A frequently used scanner will also experience aging in its piezoelectric controls. As repeated voltage is being applied throughout every usage, more dipoles in the piezoelectric material will align themselves, causing the extension of the piezo to be larger than what was initially calibrated. All the above-mentioned sources of error from the nature of a piezo electric material will contribute to our measurement of the polystyrene sphere size to defer from its realistic value.

Conclusion

The Nanotec STM provided abundant detail of the surface topography of gold islands on HOPG substrate in the micrometer scale. Voltage spectroscopy without feedback on gold and HOPG sites obtained consistent values of surface contact potential. The values obtained from voltage spectroscopy are not quite comparable to the theoretical value calculated from known work functions of gold, HOPG, and silicon. We proposed that, if clean samples can be scanned in a controlled environment, ideally vacuum, this spectroscopic method can then become more reliable in determining the work function of a material. Furthermore, voltage spectroscopy under the constant force regime were able to provide qualitative and quantitative characterization of the spherical tip shape from the distance voltage curves before it was crushed during the last measurement. It is a powerful method that can be able to provide quality control of the tip shape throughout the experiment without changes to the microscopy set up. After the crash occurred to our tip, it was unable to give us spectroscopic details of a single point. However, we are still able to use it in the contact regime to scan the surface typography of gold islands deposited on Si (111) substrate with remarkable clarity. These results and observations are evident in that tip shape as well as precision are crucial in spectroscopic measurements of point sites, but general surface mapping without achieving atomic resolution can still be obtained carefully with tip defect.

References:

[1] P. Eaton and P. West, "Introduction," in *Atomic Force Microscopy*, Oxford: Oxford University Press, 2010. doi: 10.1093/acprof:oso/9780199570454.003.0001.

[2] G. Binnig, C. F. Quate, and Ch. Gerber, "Atomic Force Microscope," *Phys. Rev. Lett.*, vol. 56, no. 9, pp. 930–933, Mar. 1986, doi: 10.1103/PhysRevLett.56.930.

[3] "Atomic Force Microscopy (AFM)." Freie Universität Department of Physics.

[4] "SPM Techniques." Freie Universität Department of Physics.

[5] J. Lü *et al.*, "Surface potential studies using Kelvin force spectroscopy," *Appl. Phys. Mater. Sci. Process.*, vol. 66, no. 7, pp. S273–S275, Mar. 1998, doi: 10.1007/s003390051144.

[6] L. Olsson, N. Lin, V. Yakimov, and R. Erlandsson, "A method for in situ characterization of tip shape in ac-mode atomic force microscopy using electrostatic interaction," *J. Appl. Phys. - J APPL PHYS*, vol. 84, pp. 4060–4064, Oct. 1998, doi: 10.1063/1.368618.

[7] "NANOTEC SPM User Manual." Freie Universität Department of Physics.

[8] W. M. H. Sachtler, G. J. H. Dorgelo, and A. A. Holscher, "The work function of gold," *Surf. Sci.*, vol. 5, no. 2, pp. 221–229, Oct. 1966, doi: 10.1016/0039-6028(66)90083-5.

[9] W. N. Hansen and G. J. Hansen, "Standard reference surfaces for work function measurements in air," *Surf. Sci.*, vol. 481, no. 1, pp. 172–184, Jun. 2001, doi: 10.1016/S0039-6028(01)01036-6.

[10] J. Lindmayer, "Field effect studies of the oxidized silicon surface," *Solid-State Electron.*, vol. 9, no. 3, pp. 225–235, Mar. 1966, doi: 10.1016/0038-1101(66)90107-9.